Level Set based Tracking for Cell Cycle Analysis using Dynamical Shape Prior

Yan Nei Law
lawyn@bii.a-star.edu.sg
Hwee Kuan Lee
leehk@bii.a-star.edu.sg

Bioinformatics Institute
30 Biopolis Street, #07-01 Matrix,
Singapore 138671

Abstract

Automated cell tracking in populations is very crucial for studying dynamic cell cycle behaviors. However, high accuracy of each step is essential to avoid error propagation. In this paper, we propose an integrated three-component system to tackle this problem. We first model the temporal dynamics of shape change using an autoregressive model, which is used for estimating the shape and the location of the current object. We then segment the cell using active contour model starting from the predicted shape. Finally, we identify its phase using Markov model. This information is also used for further fine-tuning the segmentation result. We applied this approach for tracking HeLa H2B-GFP cells and high accuracy validation results confirm the usefulness of our integrating approach.

1 Introduction

To study dynamic cell cycle behaviors [6], single cell tracking in populations is a crucial step to obtain quantitative measurements. In many studies, this process was carried manually which is very time-consuming and the results could be subjective. To automate this process, we introduce a new system for individual cell tracking in this paper. The system shown in Fig. 1 consists of three components: (C1) Learning shape prior for tracking, (C2) Segmentation using prior, and (C3) Cell phase identification. In contrast with most of the existing methods which focused on these subproblems separately, this approach makes use of available biological prior knowledge for improving the performance of the whole process.

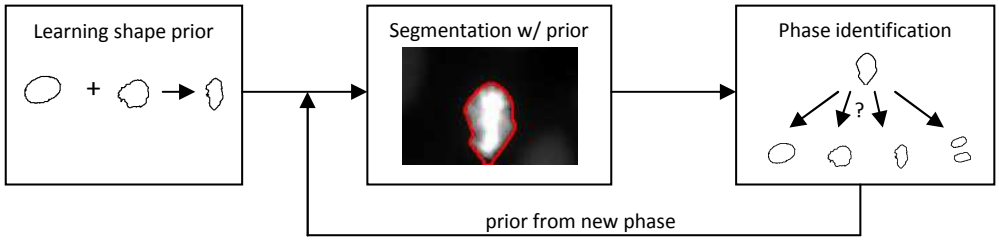

Figure 1: Flowchart of the proposed system.

For (C1), we model the temporal dynamics of shape change using an autoregressive model [1, 4, 7]. To obtain a more reliable model, we use a low-dimensional formulation

to represent a shape. The model is used for estimating the shape and the location of the current object. Details will be present in Section 2. For (C2), we use initialization from (C1) and segment the cell using an active contour model [5]. This step greatly improves the segmentation accuracy. Details will be present in Section 3. For (C3), we model this using Markov process and classify the segmented cell. The segmentation result is further enhanced based on a given sample shape if the cell undergoes a phase transition. Details will be present in Section 4. Note that our approach is very generic and can be applied for a large variety of cell images by using different training examples and sample shape examples.

2 Learning Shape Prior for Tracking

2.1 Finite-dimensional curve representation

Given a sequence of N training shapes, we define the centroid as the center of mass and the orientation as the angle between the horizonal axis and the major axis of the ellipse that has the same second-moments as the shape. After a suitable transformation, all the shapes are centered and have 0 orientation. Their signed distance functions (SDFs) $_1$ $_N$ are uniquely determined [4]. The mean shape $_0$, is computed by taking the mean of the SDFs, $_0$ $\frac{1}{N}$ $_i$. The n largest eigenmodes $_1$ $_n$ with n N are computed by Principal Component Analysis (PCA) [2]. Then each training shape can be approximated by a linear combination of the eigenmodes:

$$_i\,x \quad _0\,x \quad \sum_{j\ 1}^{n} \quad _{ij}\ _j\,x$$

where $_{ij}$ $_i$ $_0$ $_j$ $_i\,x$ $_0\,x$ $_j\,x$ dx. This representation has been widely used for constructing shape priors [1, 4]. Given an arbitrary shape (after a suitable transformation), it can be approximated by a shape vector of the form $_0$ $_1$ $_0$ $_n$. For the transformation parameters (translation and rotation), instead of using the absolute transformation , we use the incremental transformation , i.e., difference between the current transformation and the previous transformation. Together with the shape parameters, a sequence of shapes can be represented by a sequence of combined vectors

$$\mathbf{v}_i \qquad \begin{matrix} i \\ i \end{matrix} \tag{1}$$

The main advantages of this representation are its simplicity and robustness.

2.2 Learning temporal dynamics of shape change

Given the shape and transformation parameters $\mathbf{v}_1$ $\mathbf{v}_{t\ 1}$ obtained from the previous shapes $_1$ $_{t\ 1}$, we aim to estimate the parameters of the shape at time t. To achieve this, we model this process using an autoregressive model (AR) of order 2 [7], i.e.,

$$\mathbf{v}_t \qquad A_1\mathbf{v}_{t\ 1} \quad A_2\mathbf{v}_{t\ 2} \tag{2}$$

where is the mean and is zero-mean Gaussian noise with covariance . To estimate the model parameters, we use a stepwise least squares method proposed in [7]. We then predict the shape vector $\mathbf{v}_t$ as $\tilde{\mathbf{v}}_t$ $A_1\mathbf{v}_{t\ 1}$ $A_2\mathbf{v}_{t\ 2}$. Since the estimation provides information about the shape and the location of the current object, this serves as a purpose of tracking embedded into the system. Figure 2 shows the approximation of a HeLa cell in each phase.

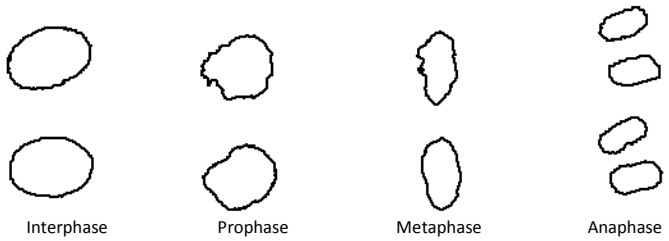

Figure 2: The approximation (below) of a cell (above) by the first six principal components.

3 Segmentation with shape prior initialization

Given an image I_t : **R** and a sequence of previous segmented images, our aim is to track the object in I_t making use of the information derived from the estimated shape vector $\tilde{\mathbf{v}}_t$, which is often very accurate. In image processing applications, many effective active contour models [8] require a good initialization. The estimated shape $\tilde{\mathbf{v}}_t$ we generated can serve this purpose well.

To segment the object, we choose the edge-based active contour model proposed in [5] among many segmentation methods [8] because it inherits some advantages of level set methods such as simple representation for contours of complex topology and simple numerical computations on regular grids, while it has an intrinsic capability of maintaining regularity of the level set function. The objective is to find a level set function : **R** such that the following energy functional F is locally minimized:

$$F \quad a \quad p \quad dx \quad b \quad g \quad dx \quad c \quad gH \quad dx \tag{3}$$

where a b 0 and c **R** are the coefficients of the three terms, p is a potential function, g is an edge indicator function, and H are the Dirac delta function and the Heaviside function respectively. Here, we use

$$p\ s \quad \begin{array}{ll} \frac{1}{2^{\ 2}}\ 1 \quad \cos\ 2\ \ s & \text{if } s \quad 1 \\ \frac{1}{2}\ s \quad 1\ ^2 & \text{if } s \quad 1 \end{array} \qquad g \quad \frac{1}{1 \quad G \quad I_t\ ^2}$$

where G is a Gaussian kernel with a standard deviation . To minimize Eq. (3), we apply gradient descent method. We denote by $\frac{F}{}$ the (Gâteaux) derivative of F with respect to . Then, a single step of the gradient descent method computes the next iterate by the update $^{k\ 1} \quad ^{k} \quad t\frac{F}{}\ ^{k}$, where t 0 is the step length parameter. The detailed numerical implementation can be found in [5]. Presumably, the contour stops at the object's boundary.

4 Cell phase identification

In this section, we identify the cell phase S_t based on the segmentation result obtained by the previous step. Here, we model this as a maximum-a-posteriori (MAP) problem. Such an approach has been widely used for modeling state transition [9, 10]. Given the current image I_t and the previous phases $S_{1:t\ \ 1} \quad S_1 \quad S_{t\ \ 1}$, we denote by $P\ S_t\ I_t\ S_{1:t\ \ 1}$ the posterior probability of the current phase S_t. Then its maximizer S_t will be the optimal current phase. Based on the Bayesian formula, the expression can be rewritten as

$$P\ S_t\ I_t\ S_{1:t\ \ 1} \quad \frac{P\ I_t\ S_t\ S_{1:t\ \ 1}\ P\ S_t\ S_{1:t\ \ 1}}{P\ I_t\ S_{1:t\ \ 1}} \quad P\ S_t\ S_{t\ \ 1}\ P\ I_t\ S_t$$

The last expression is based on the assumptions that I_t and $S_{1:t\ 1}$ are uncorrelated and S_t depends only on the previous phase $S_{t\ 1}$. For simplicity, we consider the "left-right" model, i.e., transitions could happen only between consecutive phases. Also, we track the cell in one cycle. Moreover, the probabilities of all possible transitions are equal. These assumptions could be expressed using the following matrix:

$$\begin{array}{c|cccc} & I & P & M & A \\ I & \frac{1}{2} & \frac{1}{2} & 0 & 0 \\ P & 0 & \frac{1}{2} & \frac{1}{2} & 0 \\ M & 0 & 0 & \frac{1}{2} & \frac{1}{2} \\ A & 0 & 0 & 0 & 1 \end{array}$$

where $I\ P\ M\ A$ represent interphase, prophase, metaphase and anaphase, respectively. For the likelihood function $P\ I_t\ S_t\ $, we use the following similarity measure between the segmented shape and the sample shape $_S$ associated with S where $S\quad I\ P\ M\ A\ $:

$$P\ I_t\ S_t\quad D\quad _S\quad \exp\quad _i\quad f^i\quad f^i{}_S$$

where f is the shape and context features. Here, we use eight features suggested in [10]: maximum intensity, minimum intensity, standard deviation of intensity, mean intensity, length of major axis, length of minor axis, perimeter and compactness (perimeter^2/(4 Area)).

The phase information can be used to enhance the segmentation result. If the cell undergoes a phase transition, we repeat the segmentation step with the sample shape of the new (optimal) phase as an initial guess. The sample shape is first transformed to obtain the same centroid and orientation with the segmented shape. With this biological prior knowledge, the segmentation result could be further improved by this additional step. This will be illustrated in the experimental section.

We then use the final segmented shape to compute the shape vector $\mathbf{v}_t$ and use it for predicting the shape prior for the next image.

5 Experimental results

In this section, we evaluate the performance of the proposed method empirically in various aspects: 1) temporal sampling rate, 2) system combination and 3) dwelling time.

The cells used in this paper are HeLa H2B-GFP cell line from [3] and [10] under different conditions. Frames were acquired at 3-minute intervals and 15-minute intervals respectively, with a time-lapse fluorescence microscopy. Each image is of 97 130 pixels.

To estimate the parameters of the model in Eq. (2), we manually segmented a sequence of 66 training images of a cell nucleus and computed the corresponding shape vectors and the eigenmodes (n 6) described in Section 2. For the initial setting $\mathbf{v}_1$ and $\mathbf{v}_2$ in Eq. (2), we first manually segment the first two images in the test sequence and compute their shape vectors $\mathbf{v}_1$ and $\mathbf{v}_2$.

The percentage intersection between the manual and the computed segmentation is used as a measure of segmentation accuracy and the mean accuracy with error bar is reported. The error bar indicates the standard deviation of the accuracy.

5.1 Sampling rate

In this test, we use a sequence of 40 images of cell nuclei as the test set. From this sequence, we generate four other sequences by duplicating or skipping images to simulate sequences

with higher or lower sampling rate respectively. Figure 3A shows the mean accuracy of the segmentation results vs. the temporal sampling rate. Observe that the accuracy remains high as the sampling rate is higher than 1. However, it degrades slightly when the rate is decreased. It shows that it is difficult to capture a dramatic change in shape due to low sampling rate stream. But the overall accuracy is still high. Thus, our algorithm is robust.

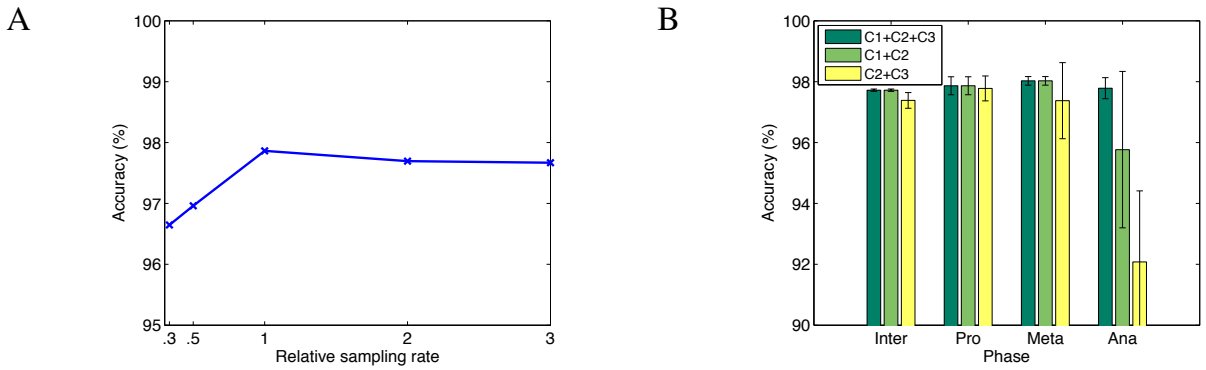

Figure 3: Mean accuracy (A) vs. sampling rates (B) with different system combinations of (C1) learning prior, (C2) segmentation and (C3) phase identification.

5.2 System combination

To evaluate the usefulness of components (C1) learning prior and (C3) phase identification, we segment the above image sequence using different system combinations. Figure 3B shows the mean accuracy of the segmentation results in different phases. For the combination of (C2)+(C3), we use the final segmentation from one frame as the initialization of the next. Observe that the accuracies in the first three phases are comparable. However, the accuracy in the anaphase is degraded when either the step (C1) or (C3) is absent. Note that the morphological change from metaphase to anaphase is dramatic. Both the initialization learned from the dynamical model and that assigned by phase identification improve significantly the results.

5.3 Image sequence with short dwelling time of prophase

In this test, we use two other sequences of 20 images of cell nuclei having different sampling rates (A: low, B: high). For these two sets, the cells have a very short dwelling time of prophase which makes phase identification more difficult. Figure 4 shows the mean accuracy and some resulting images from the two sets in different phases. Observe that a short dwelling time of prophase causes a miss of metaphase identification. The error also propagates to the next phase. The effect is shown in the result of set A. However, due of its higher sampling rate, there are more frames sampled in metaphase in set B and hence is able to reduce the effect. Overall, the accuracy in anaphase is lower than that in the other phases.

6 Conclusion

In this paper, we introduced a three-component system for individual cell tracking in populations. This approach makes use of available biological prior knowledge to improve the performance of the process. On the other hand, it is very generic and can be applied for a large variety of cell images by using different training examples and sample shape examples. While we only tested the method on tracking single cells, it is natural to generalize the system by using several level set functions for multiple cell tracking. A promising future work is to optimize the performance of the integration approach to make it more practical.

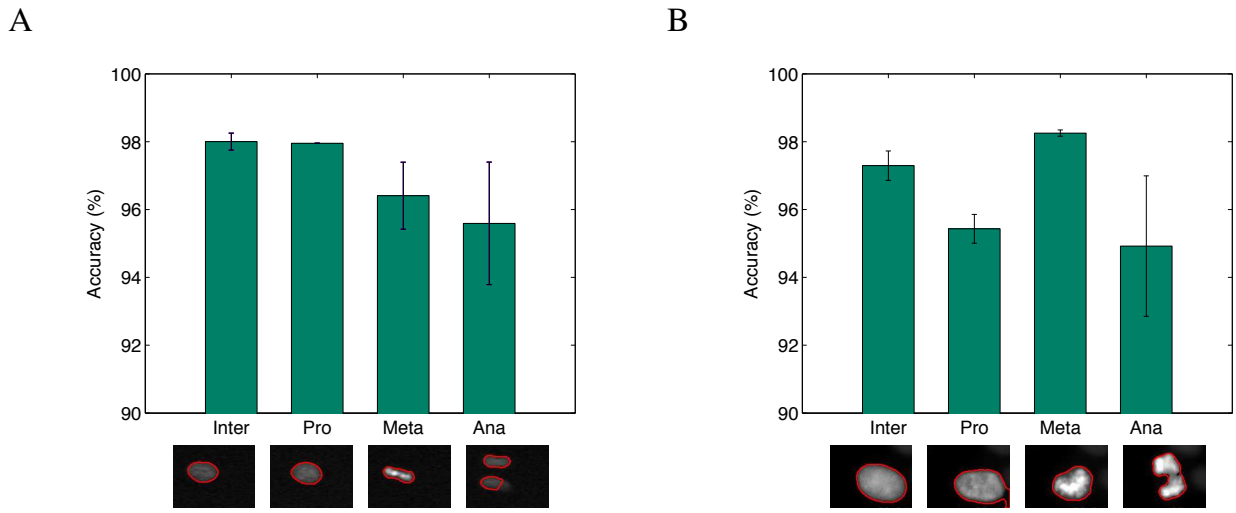

Figure 4: Mean accuracy and some resulting images in different phases.

Acknowledgement

This work was supported (in part) by the Biomedical Research Council of A*STAR (Agency for Science, Technology and Research), Singapore.

References

[1] D. Cremers. Dynamical statistical shape priors for level set-based tracking. *IEEE Trans. Pattern Anal. Mach. Intell.*, 28(8):1262–1273, 2006.

[2] R. Duda, P. Hart, and D. Stock. *Pattern Classification*. John Wiley & Sons, NY, 2001.

[3] S. Elowe, K. Dulla, A. Uldschmid, X. Li, Z. Dou, and E.A. Nigg. Uncoupling of the spindle-checkpoint and chromosome-congression functions of BubR1. *J. Cell Sci.*, 123.

[4] M. Leventon, W. Grimson, and O. Faugeras. Statistical shape influence in geodesic active contours. In *Proc. CVPR*, pages 316–323, 2000.

[5] C. Li, C. Xu, C. Gui, and M.Fox. Distance regularized level set evolution and its application to image segmentation. *IEEE Trans. Image Process.*, 19(12):3243–3254, 2010.

[6] H. Lodish, A. Berk, S. Zipursky, P. Matsudaira, D. Baltimore, and J. Darnell. *Molecular Cell Biology*, chapter 13. W.H. Freeman & Co., 2000.

[7] A. Neumaier and T. Schneider. Estimation of parameters and eigenmodes of multivariate autoregressive models. *ACM Trans. Math. Software*, 27(1):27–57, 2001.

[8] O. Scherzer. *Handbook of Mathemtical Methods in Imaging*. Springer, 2011.

[9] X. Zhou, X. Li, and W. Hu. Level set tracking with dynamical shape priors. In *Proc. ICIP*, pages 1540–1543, 2008.

[10] X. Zhou, F. Li, J. Yan, and S. Wong. A novel cell segmentation method and cell phase identification using markov model. *IEEE Trans. Info. Technol. Biomed.*, 13(2):152–157, 2009.